



# Properties of Local Oscillations in the Lower Sunspot Atmosphere

Robert Sych<sup>1</sup> , Yuzef Zhugzhda<sup>2</sup>, and Xiaoli Yan<sup>3</sup>

<sup>1</sup> Institute of Solar-Terrestrial Physics SB RAS, Irkutsk 664033, Russia; [sych@iszf.irk.ru](mailto:sych@iszf.irk.ru)

<sup>2</sup> Pushkov Institute of Terrestrial Magnetism, Ionosphere and Radio Wave Propagation RAS, Troitsk 108840, Russia

<sup>3</sup> Yunnan Observatories, Chinese Academy of Sciences, Kunming 650011, People's Republic of China

Received 2019 August 28; revised 2019 November 19; accepted 2019 November 20; published 2020 January 10

## Abstract

We present a study of wave processes in the sunspot region NOAA 12670 on 2017 August 10 observed by the Goode Solar Telescope in the TiO 7057 Å and H $\alpha$  6563 Å spectral lines. To study the distribution of power oscillations and their dynamics, we applied the pixelized wavelet filtering technique. For the first time, we obtained the spatial structure of oscillation sources as the footpoints of fine magnetic tubes, anchored in the sunspot umbra. We found that at the chromosphere level, the variation of emission is a combination of numerous independent oscillations located in the sources with small angular size. Their spatial shape varies from dots and cells in the umbra to filaments in the penumbra. Each narrow spectral harmonic corresponds to its source, without global correlation among themselves. There is a weak background as low-frequency oscillations distributed over the whole umbra. At the photosphere level we found regions with co-phased broadband oscillations of the whole umbra. Their spectrum includes the  $\sim 3$  minutes harmonic, whose maximal value is localized in umbral dots, and the low-frequency part near a period of  $\sim 5$  minutes. It is shown that the oscillation sources are displaced at different heights with increasing angular size. We assume that the observed spatial distribution of wave sources indicates the existence of a slow subphotospheric resonator with a vertical magnetic field in the umbra and a wave cutoff frequency due to inclination of the magnetic field line in the penumbra.

*Unified Astronomy Thesaurus concepts:* Sunspot groups (1651)

## 1. Introduction

The first observations of sunspot oscillations (Beckers & Tallant 1969; Wittmann 1969) showed that they are most pronounced in the core of Ca II chromospheric lines as so-called umbral flashes (UFs). This phenomenon was studied in a number of papers (Kneer et al. 1981; Turova et al. 1983; Socas-Navarro et al. 2000; López Ariste et al. 2001; Rouppe van der Voort et al. 2003; Nagashima et al. 2007; Tziotziou et al. 2007). UFs are also associated with the phenomenon of running waves in the penumbra, which is observed in the H $\alpha$  and He lines (Bloomfield et al. 2007) as well as Ca II (de la Cruz Rodríguez et al. 2013) as symmetric spatial structures moving in the radial direction from the umbral center to the outer boundary of the penumbra (Tsiropoulou et al. 2000; Rouppe van der Voort et al. 2003). Propagating waves are non-stationary, with a change in the power of oscillations, both in time and in space (Sych et al. 2010). This leads to a significant periodic modulation of the propagating 3 minutes waves. A possible response of such modulation is the appearance of both low-frequency wave trains and emission from separate brightening maxima as UFs in the footpoints of the magnetic tubes (Sych & Wang 2018).

According to Bel & Leroy (1977), the low-frequency waves generated at the subphotospheric level (p-mode) propagate through the natural waveguides as a concentration of magnetic elements—sunspots and pores. Their oscillation period can be modified by the wave cutoff frequency. It is shown (Bel & Leroy 1977; Zhugzhda & Dzhililov 1984) that oscillations with a frequency below the magnetoacoustic cutoff frequency are quickly damped. The main factor affecting the cutoff frequency is the inclination of the field lines where the wave propagation is observed. Thereof, we observe 5 minutes oscillations in diverging magnetic fields both in the chromosphere (spicules, De Pontieu et al. 2004) and in the corona

(loops of active regions, De Pontieu et al. 2005; de Wijn et al. 2009). The study of low-frequency oscillations in the upper levels of the solar atmosphere (Marsh et al. 2009; Wang et al. 2009; Yuan et al. 2011) confirmed the assumption that their appearance at such heights is a consequence of channeling waves in inclined magnetic fields. The observed propagation speed of the disturbances indicates their nature as slow magnetoacoustic waves (Sych et al. 2009; Kiddie et al. 2012).

It was assumed that oscillations in sunspots originate from the penetration of 5 minutes oscillations from the convection zone. After transformation into slow MHD waves, the oscillations propagate upward into the photosphere, the chromosphere, and the corona. Spectral analysis of observations showed the presence of 5 minutes oscillations in the photosphere and 3 minutes oscillations in the chromosphere and the corona. Many numerical experiments were carried out within this approach (Khomenko & Collados 2015).

At the photosphere level the 3 minutes sunspot oscillations are very low and not visible because their amplitudes are negligible compared to the 5 minutes oscillations. For example, Balthasar et al. (1987) could not detect their manifestations at the photosphere. Nagashima et al. (2007) showed that the oscillation power at all frequencies significantly drops in the sunspot umbra. At the same time, the first information about the possibility of registering these variations appeared. In Kobanov et al. (2011a), the 3 minutes oscillations at the photosphere level were detected for the first time, and they were compared with the chromospheric data. It is shown that the localization of the maximum power of oscillations at the chromosphere level coincides in space with a minimum at the photosphere level. However, these observations with a spatial resolution of  $\sim 1''$  did not allow one to distinguish the two-dimensional structure of the oscillation sources. The 3 minutes oscillations were interpreted in the framework of the

chromospheric resonator hypothesis. But observations (Zhugzhda 1984; Settele et al. 2001) questioned this hypothesis by taking into account the presence of local oscillations. The central problem was the presence of powerful local 3 minutes oscillations detected in the umbral dots (UDs) at the photosphere level (Jess et al. 2012; Ebadi et al. 2017).

In the chromosphere, oscillations become visible due to filtering of the 5 minutes oscillations and a sharp decrease in plasma density compared to the photosphere. Local 3 minutes oscillations cannot be explained in the framework of the hypothesis about penetration and transformation of the p-mode oscillations. This is because p-modes effectively transform only into large-scale oscillations covering the whole sunspot and not into small-scale local oscillations (Zhugzhda & Sych 2014). This has been shown within the monolithic sunspot model. Within the cluster sunspot model comprising a set of separated magnetic tubes, it is impossible to explain the local 3 minutes oscillations. The absorption of p-modes in magnetic tubes is greatly weakened, which is considered to be a reason for the weakening disturbances in sunspots compared to the surrounding solar atmosphere (Jain et al. 2014). This absorption rapidly decreases with frequency, which excludes the presence of powerful local 3 minutes oscillations at the photosphere level.

Zhugzhda & Dzhililov (1984) and Zhugzhda & Sych (2014) proposed an alternative model of local oscillations, based on the possibility of the existence of a subphotospheric resonator for slow waves. An excellent candidate for structures where the resonance is possible through convective jets (plumes) in the sunspots was found in the set of numerical experiments (Schüssler & Vögler 2006). These jets lead to the emergence of UD, where the 3 minutes oscillations were detected. The proposed model brings together such key problems of sunspot theory as the convective energy transfer in sunspots, the presence of umbral bright dots, 3 minutes oscillations, powerful brightening as UFs, and active phenomena in the chromosphere and the sunspot corona under the UF effect.

In this paper, we analyze the fine spatial structure of wave sources in sunspots obtained at the photosphere and chromosphere levels, and examine its relationship with active energetic phenomena such as UFs and UD. The pixelized wavelet filtering (PWF) technique was used for spatial localization of the sources. The article is structured as follows: in Section 1 we introduce the topic and present the objects of study; in Section 2 we describe the observations and data processing; Section 3 presents the data analysis with results and discussion on the physical processes connected with the considered wave phenomena at different heights; Section 4 contains our conclusions from the obtained results.

## 2. Observations and Data Processing

The two optical channels centered on the  $H\alpha$  line core (6563 Å) and TiO (7057 Å) of the Goode Solar Telescope (GST) (Cao et al. 2011), located at the Big Bear Solar Observatory (BBSO), were used to observe chromospheric and photospheric images of the active sunspot region NOAA 12670 (S06 W47) on 2017 August 10 (18:18–19:11 UT). The atmosphere conditions during observations were very good and stable. The observations were carried out using a high-order adaptive optical system with 308 sub-apertures. We used the Broadband Filter Imager for obtaining the TiO data and the Visible Imaging Spectrometer for obtaining the  $H\alpha$  data. The field of view of both instruments is 70". The pixel scale is

0".0295 for the  $H\alpha$  center and 0".0342 for the TiO images with spatial resolutions of 0".1 and 0".11 respectively. The TiO filter is an interference one, and its bandpass is 10 Å. Thus, the TiO band is  $7057 \text{ Å} \pm 5 \text{ Å}$ . For the  $H\alpha$  line combination a 5 Å interference filter and a Fabry–Perot etalon give a 0.07 Å bandpass. To obtain more spectral information, we scan the  $H\alpha$  line at seven wavelength points: 0.0,  $\pm 0.4$ ,  $\pm 0.8$ , and  $\pm 1.0 \text{ Å}$ . The exposure times of  $H\alpha$  images were 7, 9, 15, and 20 ms respectively. The cadence is 18 s for the  $H\alpha$  images and 13 s for the TiO channel.

Observation using instrumental filters allows us to obtain information from the narrow layers of a sunspot's atmosphere with an opacity effect when comparing the origin of sunspots at different heights. This effect is important for narrowband sources because their visibility can vary with wavelength and bandwidth. For broadband waves of sunspots that propagate from the subphotospheric layers into the corona, the effect of the brightness variation depends mainly on the inclination of the magnetic field line, and accordingly the cutoff frequency. Changing the wavelength in the filter bandwidth will not play an important role, since the wave process occupies the whole sunspot atmosphere and will be visible in the entire band simultaneously.

In the first stage of data preparation, the images were adjusted to correct the rotation of the telescope platform during observations. Then we aligned the images using the fast Fourier transform (FFT) method to maximize the cross-correlation of the images with respect to the reference image. According to the results of FFT preparation, images were shifted relative to each other. All data have been corrected using standard software provided by the BBSO.

We applied the PWF technique (Sych & Nakariakov 2008) for spectral data preparation. This method was previously widely used by authors in studies of sunspot oscillations (Sych et al. 2010, 2015; Sych & Nakariakov 2014; Sych & Wang 2018). The numerical method is a generalization of the wavelet transform of 3D data cubes. The temporal signal of each spatial pixel is wavelet-transformed with a Morlet mother function (Torrence & Compo 1998), which results in 4D data cubes for power, amplitude, and phase (two spatial dimensions, time, and frequency). The obtained data can be processed according to a specific request. For example, selecting a certain spectral component or integrating over a certain narrow spectral range makes a 3D narrowband data cube that consists of a sequence of narrowband maps.

We reconstructed the time signals using a spectral filter as a running window with the narrow band from  $P_i/1.25$  to  $P_i \times 1.25$ , and steps of 0.1 minute, where  $P_i$  is the current value of the period. The range of periods was from 1 minute to 8 minutes. For each reconstructed signal, the values of amplitude variations were calculated. Repeating a similar procedure for all image points, we prepared a series of surfaces as narrowband images of oscillation sources. To show the global 1D spatial dependence of the period along the selected spatial axis, we scanned the narrowband sunspot images and prepared a coordinate–period diagram. A similar technique was applied in Sych & Nakariakov (2014) to study oscillations using *SDO/AIA* data in the UV range.

To conveniently present radially propagating wave fronts, and to calculate their spectral characteristics, all sunspot images were rotated counterclockwise by  $12^\circ$  for vertical positioning. The space-averaged coordinate–period diagrams were obtained,

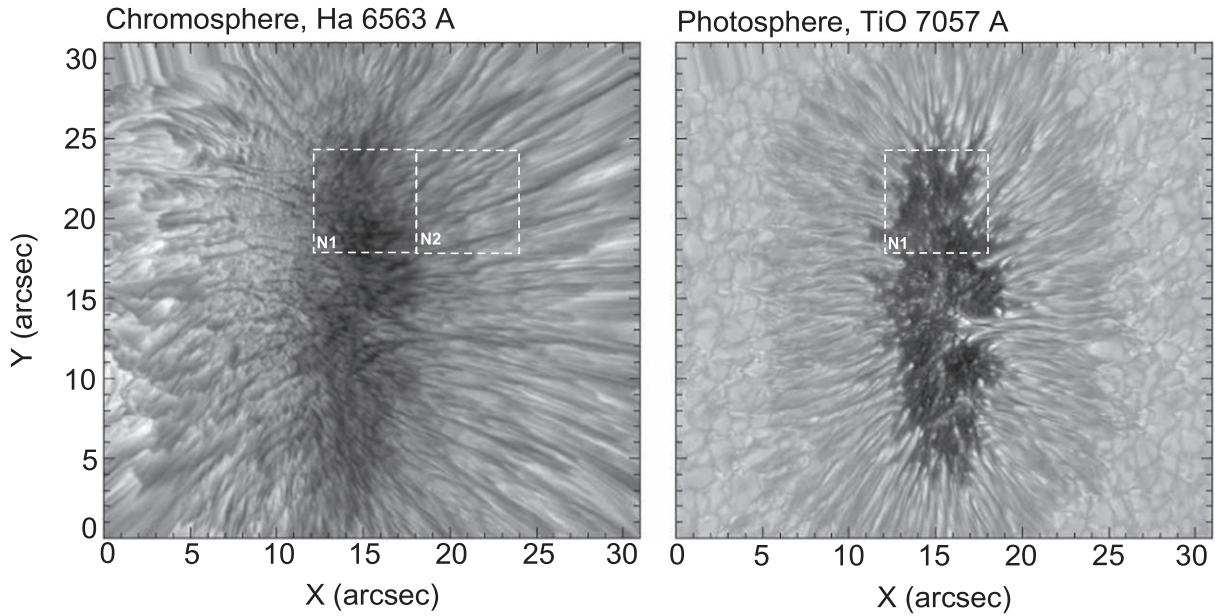


**Figure 1.** Image of the active sunspot group NOAA 12670 on 2017 August 10 at 18:18 UT, obtained with the GST at BBSO in the  $H\alpha$  6563 Å line (left panel) at the chromosphere level, and in the TiO 7057 Å line (right panel) at the photosphere level. White numbered rectangles indicate the studied areas, N1 and N2. Brightness is on a log scale. Spatial coordinates are in arcseconds.

which allowed a 1D distribution of the oscillation sources to be obtained. To localize their positions in space, we also obtained the 2D structure as an image with calculated oscillation periods and power.

Based on the PWF technique, we developed a method of preparing color maps of period and power. For each spatial point of a narrowband image cube, we constructed the period profiles and calculated their spectral peak and corresponding period oscillations. We assumed that these values should be no less than half of the maximum spectral power in a given period band. The points with the maximum power of oscillation were selected using a certain color in accordance with the color table. This table defines the specified sequence of color depending on the periods. The points with a spectral peak below the specified level were chosen as zero, with no oscillations, and not displayed on the color map. Details obtained as repeating points of the same color from oscillation sources with the same period. A similar mapping method was previously developed in Nakariakov & King (2007) by using Fourier transforms for spectral decomposition of signals.

### 3. Results and Discussion

Figure 1 shows images of the active sunspot group NOAA 12670 obtained on 2017 August 10. The observations start at 18:18 UT and their duration is 53 minutes. The spatial details in the  $H\alpha$  line (left panel, chromosphere) and TiO line (right panel, photosphere) show the pronounced processes of variation in emission as running waves, UFs, and bright dots. Broken squares indicate the study areas N1 (umbra) and N2 (penumbra) with an angular size of  $6'' \times 6''$ . The number of images obtained was 247 frames in the TiO line and 178 frames in the  $H\alpha$  spectral line. The duration and cadences of observation allowed identification of oscillations with periods ranging from  $\sim 1$  to  $\sim 20$  minutes.

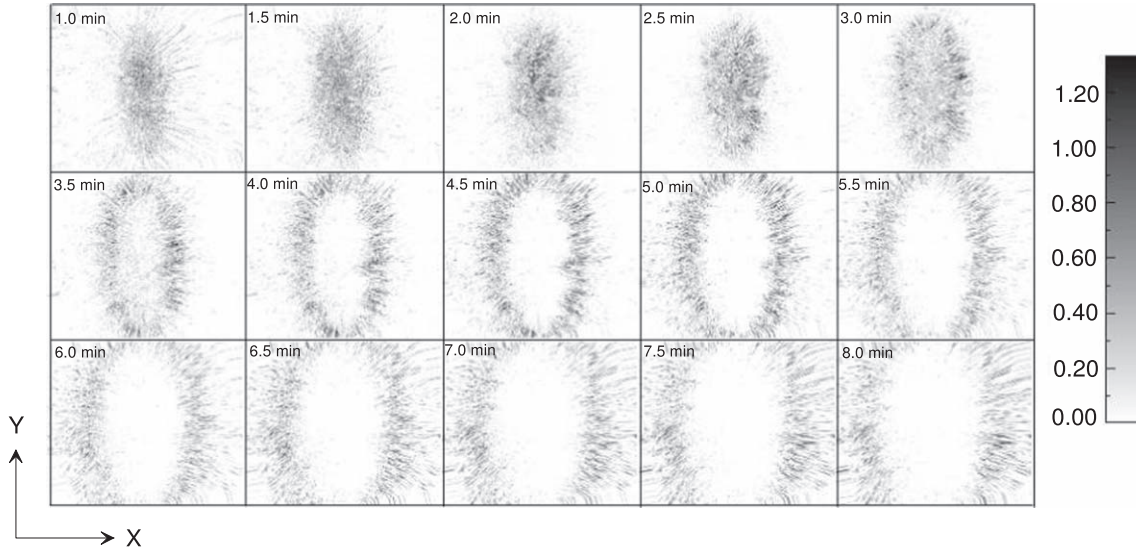
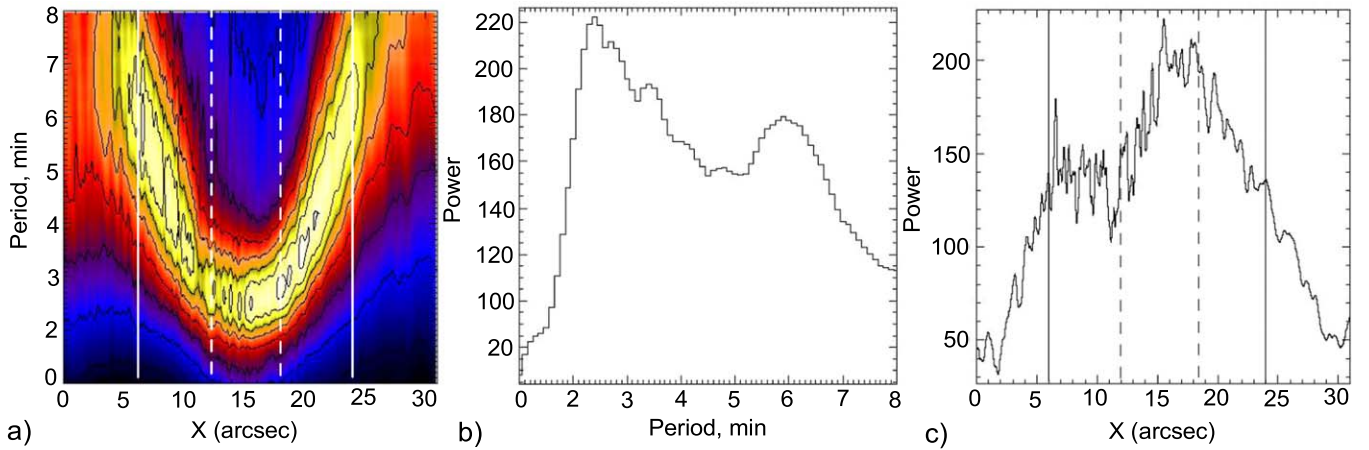
#### 3.1. 1D Fine Structure of Sunspot Oscillations

Filtering the data cubes through a running window with average intensity subtraction, we obtained a set of sunspot narrowband images as ellipses that, as the period grows, transform into expanding rings. We can see (Figure 2) that, for high-frequency oscillations at chromosphere level ( $H\alpha$ ), sources with a period of less than 3 minutes are localized in the sunspot umbra, and the area that they occupy decreases with decreasing period. This regularity agrees well with earlier studies of sunspot oscillations (Reznikova & Shibasaki 2012; Jess et al. 2012; Yuan et al. 2014). We can also see a fine structure as small dotted and extended patches that fill the central part of the umbra.

Using a set of narrowband images (Figure 2) we obtained a spectral distribution of the averaged oscillation power in the sunspot (Figures 3 and 4). For this we scanned the images along the X-axis for each point on the Y-axis. Then, the resulting set of scans was averaged. The average was performed because of spatial inhomogeneities of the oscillations. During our analysis we have excluded the upper and lower boundaries of the images from the averages. The obtained 1D scans for each period composed a coordinate–period diagram (Figure 3(a)) with spatial details like two diverging arcs of ellipse that trace the sunspot oscillation power. The angular size of these details increases with period and displaces the penumbral boundaries. This indicates the existence of diverging magnetic field lines, along which waves propagate upward, into the corona (Sych et al. 2012).

We can see (Figure 3(a)) that the high-frequency part of the sunspot oscillations is located within the umbral boundaries with  $\sim 5''$  size, marked by vertical dashed lines. Calculation of the periods where the power is maximal gave us the oscillation spectrum (Figure 3(b)). The same procedure but for coordinates gave us the spatial distribution of power oscillations (Figure 3(c)). There are two spectral peaks: one near a period of 3 minutes and the other within 5–7 minutes. For convenience,



Narrowband maps of sunspot oscillations (H $\alpha$ )**Figure 2.** Sunspot narrowband maps of oscillation power for the H $\alpha$  6563 Å wavelength. Period values are in minutes. Brightness in relative units.**Figure 3.** Spectral distribution of the oscillation power for the sunspot in the H $\alpha$  line (6563 Å, chromosphere). (a) Coordinate–period oscillation diagram. (b) Oscillation spectrum. (c) 1D spatial distribution of the sunspot oscillation power. Dashed and continuous lines show the umbral and penumbral boundaries, respectively. Oscillation periods are in minutes and spatial coordinates in arcseconds.

we will term the oscillations in the 2–4 minutes high-frequency range as the  $\sim 3$  minutes oscillations, and those in the 4–8 minutes low-frequency range the  $\sim 5$  minutes oscillations. The maximal power in the umbra is related to the 3 minutes periodicity.

In Figure 3(a) we can see the sources with a small angular size of  $\sim 1''$ – $2''$ . This indicates that, even with strong averaging over the whole sunspot, a fine spatial structure is detected in the umbra with minimal angular size. In quiet regions, the low-frequency component dominates.

Processing the data similarly to at the chromosphere level, we obtain the photosphere power distribution of oscillations. Figure 4 shows the obtained coordinate–period diagram (a), oscillation spectrum (b), and spatial distribution of the spectral power (c).

Comparison of the obtained coordinate–period diagrams at different heights showed strong differences. The chromospheric maximum in the sunspot umbra (Figure 3(c)) coincides with minimum oscillations at the photosphere level

(Figure 4(c)). At the photosphere we do not observe growth of the oscillation period from the umbral center. We see (Figure 4(a)) that the oscillations have a broadband character. The main power is concentrated in a low-frequency range (Figure 4(b)), which is related to the global  $\sim 5$  minutes oscillations as a p-mode.

As we move toward the umbral center, we observe a smooth lowering of the background oscillations. This trend is clearly visible in the penumbra and has a symmetric character. Then, within the umbral boundaries, the oscillation power starts to grow over a broad range (Figure 4(a)) but for fine structures. This dependence is seen clearly on the 1D profile of the spectral power (Figure 4(c)), where the arrow marks the local increases.

We found a fine spatial structure of sources in the umbra, as well as at the chromosphere level. The oscillations do not occupy a narrow range of periods like 3 minutes sources at the chromosphere (Figure 3(a)), but a broad range extending up to 8 minutes. The shape of the sources shows a small size and stable localization. The averaged spectrum (Figure 4(b)) does

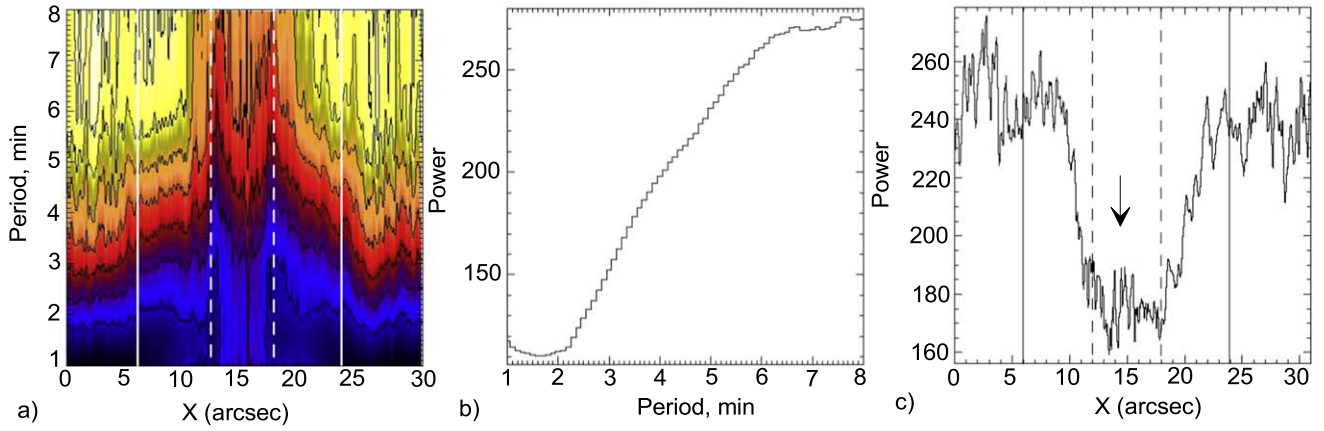


**Figure 4.** Same as Figure 3 but in the TiO line (7057 Å, photosphere). The arrow shows the increase in fine umbral oscillations.

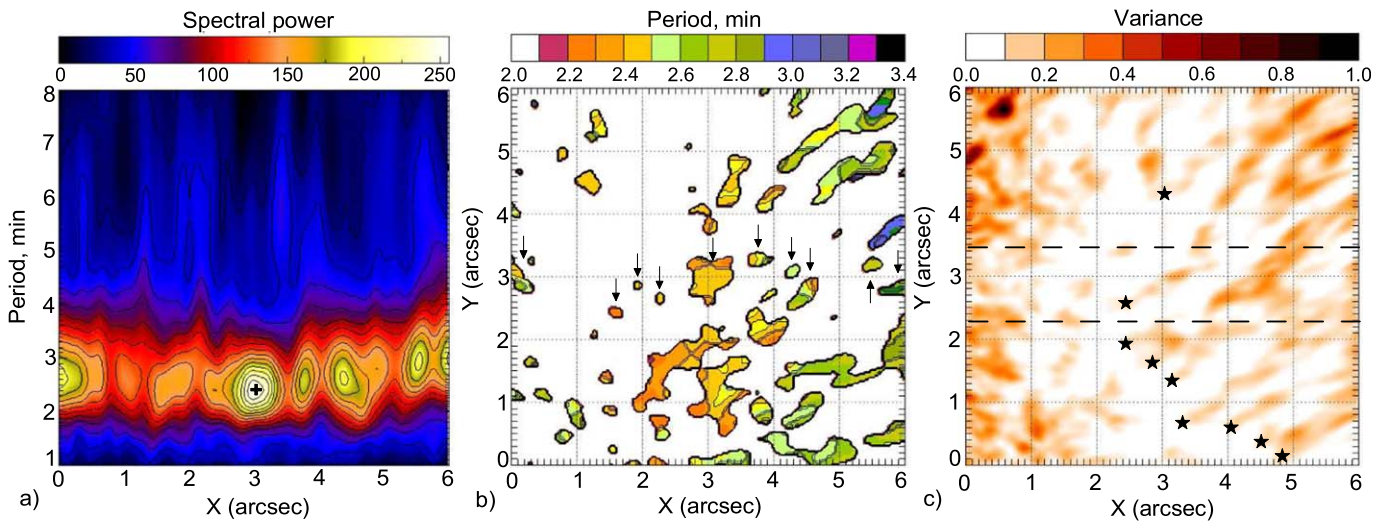


**Figure 5.** (a) 1D spectral distribution of the oscillation power (coordinate–period diagram) of area N1 in the H $\alpha$  spectral line. (b) 2D color map of the oscillation periods. (c) Variance map of the intensity oscillations. Horizontal dashed lines show the scanning region. Arrows indicate the local oscillation sources that correspond to powerful sources on the 1D diagram. The stars show the beginning of the wave paths.

not have significant oscillation peaks. There is only a growth of oscillation power with period. The umbral oscillations are very weak and not detected in the full signal.

### 3.2. Spatial Distribution and Dynamics of Oscillations

Recently the theory of 3 minutes oscillations significantly changed because of results obtained with high resolution. The oscillations are a result of the penetration of the p-mode from the surrounding quiet atmosphere into a sunspot (Khomenko & Collados 2015) as a tail of a broadband spectrum of oscillations in a quiet atmosphere. Due to the cutoff of the spectrum, only a 3 minutes periodicity remains in the temperature minimum of the chromosphere. In the photosphere, weak 3 minutes oscillations are not visible against powerful 5 minutes oscillations. However, the 3 minutes oscillations localized in small areas appeared to become visible as the spatial resolution of the observational instrument was increased (Jess et al. 2012; Zhugzhda & Sych 2014, 2018; Krishna Prasad et al. 2015; Chae et al. 2017). The obtained umbral oscillations show the different spatial and spectral localization depending on height. Studying the GST BBSO high-resolution observational data

from different heights of the sunspot atmosphere enabled us to understand this fine structure for the first time.

#### 3.2.1. Chromosphere Level

The detected structure of the oscillation sources (Figure 3(a)) was obtained by averaging power over the whole sunspot. This is not sufficient to obtain the oscillations' fine structure. To study the spatial location of the detected sources, we selected the umbral area N1 (Figure 1) with size  $6'' \times 6''$  and obtained the 1D coordinate–period diagram. To study the 2D sources, we applied the PWF technique and obtained a set of narrowband images within the period range 1–8 minutes.

Figure 5 shows the obtained coordinate–period diagram, the 2D color map for the oscillation periods, and a variance map of intensity oscillations. The horizontal dashed lines show the region of spatial scanning. The maximal periodicity is observed within the period range 2–4 minutes, with the maximum near 3 minutes (Figure 5(a)). Beyond this, the oscillation power decreases. There is a fine ( $\sim 0.2''$ – $0.5''$ ) spatial structure of local sources with some inclination of the spectral power. A similar dependence, but more expressed, is observed for the whole sunspot (Figure 3(a)). We assume that the detected fine spatial



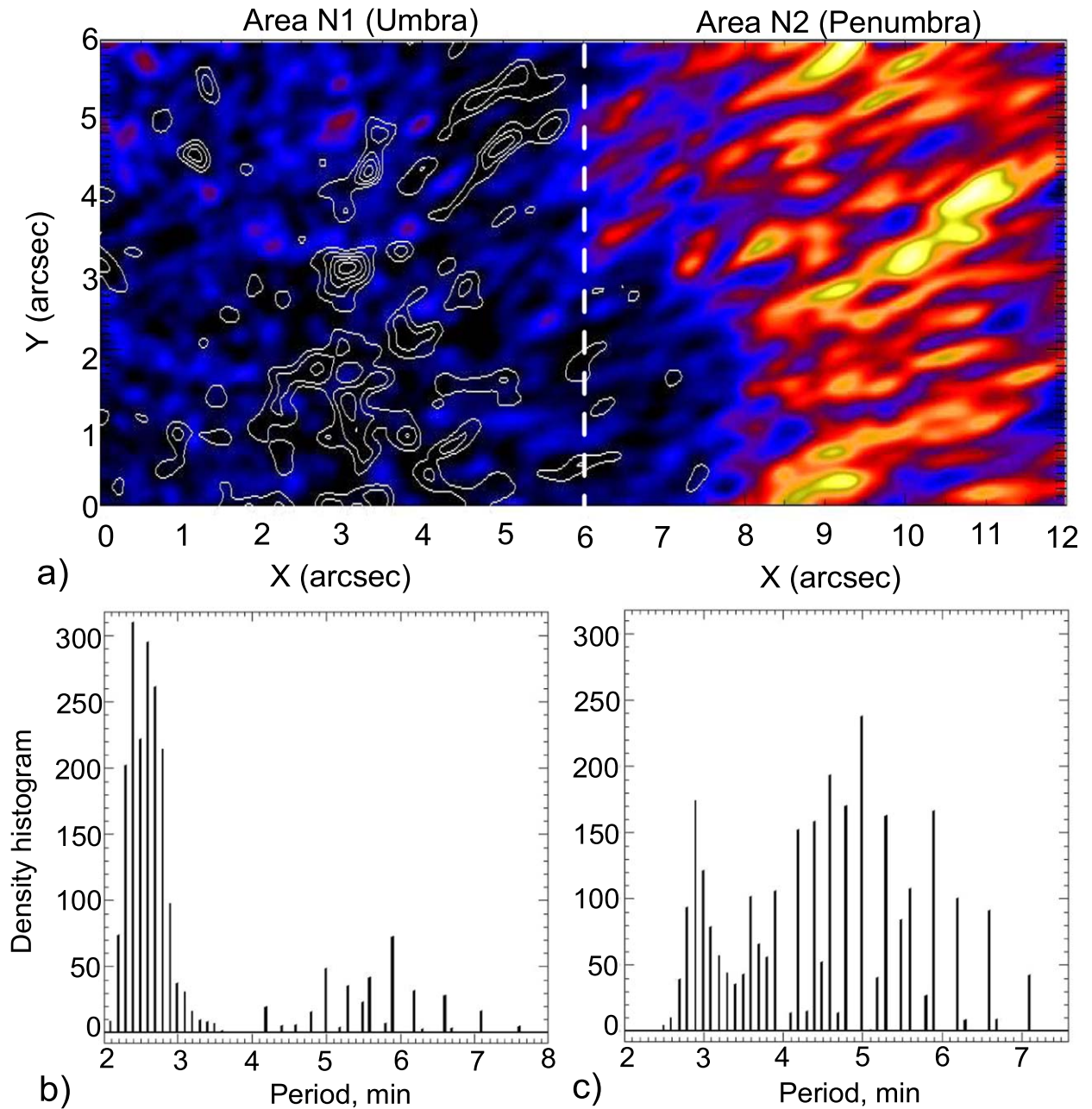


**Figure 6.** (a) Spatial distribution of power oscillations for the highlighted areas N1 and N2. The background is  $\sim 5$  minutes periodicity, and the contours are the  $\sim 3$  minutes oscillations. Histograms for the spectral density of oscillation period are shown for areas N1 (b) and N2 (c). Period values are in minutes, and the size in arcseconds.

structure is related to the sources of the  $\sim 3$  minutes oscillation harmonics.

To detect the spatial structure of the 3 minutes oscillation sources, we built a color map of the area N1 (Figure 5(b)). The level of the studied sources is limited to 50% of the power peak. We found that there is an expressed oscillation locality for all periods. The periodicity within 2–4 minutes represents a large number of independent oscillation sources with close amplitudes and periods. The arrows (Figure 5(b)) indicate bright sources within the scanning band on the coordinate–period diagram. We observed only local oscillations in the identified sources. The size of the sources with  $\sim 3$  minutes periodicity varies from  $0.2''$  to  $0.7''$ . They have a high quality factor of oscillations and a weak coupling among themselves. The waves propagate radially, along the selected directions.

The shape of sources changes from a cellular structure in the umbral center to a filament one at its boundary, as the oscillation period grows. There are both dot sources with a very narrow spectral bandwidth and extended structures such as cells and filaments. Some comprise a set of narrowband sources. The direction of the extended structures often agrees well with localization of the cellular structures.

Since the intensity of each point in the temporal data cube varies greatly in both time and space during wave propagation, we prepared a variance map (Figure 5(c)) of intensity oscillations. We found a set of elongated filamentary structures (waveguides) along which we observed the waves to propagate. The beginning of these structures coincides with the detected sources of  $\sim 3$  minutes oscillations and periodically observed bright details on the intensity map. This indicates that these

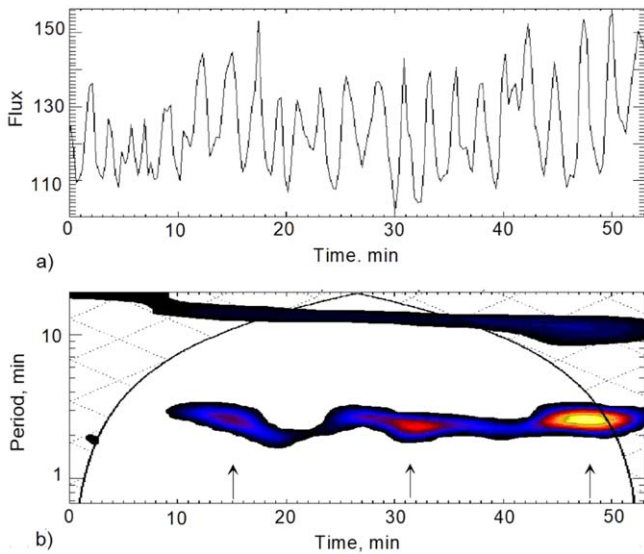


**Figure 7.** (a) Time profile of the flux variation of an oscillation source detected as a cell in the center of area N1. (b) Corresponding power wavelet spectrum. Arrows show the peaks of 3 minutes oscillation trains.

spatial details (cells or dots) are interconnected and possibly are the footpoints of thin magnetic tubes as waveguides of propagating waves.

It should be noted that the sources with small angular size, comparable with the angular resolution of the GST BBSO, are sources of periodic oscillations with a certain frequency and high power. This means that the high-frequency noise components, aperiodic in nature, will not be visible on the filtered images. All sources are well localized in space and time, and their power level is significantly higher than the noise level.

The locality of oscillation sources demonstrates not only the  $\sim 3$  minutes periodicity but also low-frequency harmonics. To study the weak umbral  $\sim 5$  minutes spectral component, we prepared a color map for the full range of variation. We chose area N2 to investigate the periodicity in the penumbra. The angular size is the same as for N1. Figure 6(a) shows narrowband images of the areas N1 (umbra) and N2 (penumbra) with their power distribution for periods of  $\sim 5$  minutes. We overlap the spectral power of the  $\sim 3$  minutes oscillations as contours. The histograms for the spectral density distribution of oscillations for each area were obtained (Figures 6(b), (c)).

We found that around 3 minutes the maximum oscillation power correlates well with the center of local cells and dot sources on the period color maps (Figure 5(b)). For extended structures, there are a few power peaks located along the sources. There are sources localized in the 5–8 minutes range, as in the 2–4 minutes range (Figure 6(a), background). The power histogram in the umbra (area N1) shows a set of narrow harmonics with periods of 2–4 minutes with a significant peak near 2.5 minutes. The power of the harmonics varies, depending on the period. Each harmonic corresponds to one or several narrowband sources presented on the period color map (Figure 5(b)). There is also a weak low-frequency part of the spectrum with a maximum near 5–6 minutes (Figure 6(b)). For area N2, the main oscillations occur around  $\sim 5$  minutes. There is also a 3 minutes peak caused by overlapping the

umbral region. The observed sources have mainly a filament shape and are placed radially from the umbral center.

Comparing the same spectral peaks shows different values in the umbra and in the penumbra (Figures 6(b), (c)). At the maximal value of the  $\sim 3$  minutes component in the umbra, its penumbral value is minimal. But, in contrast, at the minimal power of 5 minutes oscillations in the umbra, they are maximal in the penumbra. The low-frequency sources are arranged among the high-frequency ones, with no overlap. In the umbra, the sources with  $\sim 5$  minutes periodicity have a cellular structure, which smoothly transforms into a filament one in the penumbra.

To study the temporal parameters of the detected oscillations, we selected an extended source with the maximal amplitude. The cross indicates the source on the coordinate–period diagram (Figure 5(a)). This source coincided spatially with an oscillating cell having an angular size of  $\sim 0''.5$  and which is located in the center of the period color map (Figure 5(b)). Figure 7 shows the flux temporal profile obtained by integrating the studied area, and its power wavelet spectrum.

We found that non-monotonic periodic oscillations prevail in the source. To study them, we built a power wavelet spectrum with 90% significance. Figure 7(b) shows that the oscillations are concentrated within a period range of 2–4 minutes, and are modulated by three low-frequency trains. The maxima of the revealed oscillation period are  $\sim 2.5$  minutes (main oscillations) and  $\sim 13$  minutes (wave trains).

A similar spectral analysis for the dot sources showed the presence of oscillation trains, but without period drifts. There is only one oscillation frequency within the envelope curve. We can assume that the drifts in cells are caused by the dynamics of a collection of the dots with various periods, where the periods vary with time as the train power increases. For the cell we see (Figure 5(b)) several fine sources at the cell boundary, whose variation in periodicity may lead to the observed drifts. For dot sources, there is only one modulation period without drifts.

The weak oscillations within  $\sim 5$  minutes periodicity are unstable and vary with time. During the observational period, the  $\sim 3$  minutes periodicity may turn into the  $\sim 5$  minutes one. The duration of the components in the signal determines what period and power we will observe in the spectrum. For powerful  $\sim 3$  minutes oscillations in the umbral cells and for  $\sim 5$  minutes oscillations in the penumbral filament sources, we observe variations that are stable in time and period amplitude.

Figure 2 and the coordinate–period diagram (Figure 3(a)) show a symmetric increase of the oscillation period with distance from the umbral center at the chromosphere level. High-frequency oscillations are concentrated in the umbra, whereas the lower-frequency component is visible as expanding oscillating rings located in the penumbra (Figure 2(b)). A similar relation was described earlier (Sych & Nakariakov 2008; Kobanov et al. 2009; Reznikova et al. 2012; Jess et al. 2013; Yuan et al. 2014). This dependence can be interpreted as a variation of magnetic field inclination, and correspondingly as changes in cutoff frequency (Bel & Leroy 1977). The maximal power value with  $\sim 3$  minutes periodicity (Figure 3(c)) is localized within the umbral boundaries. This dependence is opposite to the umbral depression at the photosphere level (Figure 4(c)).

The 3 minutes periodicity consists of spatially separated sources having a small angular size. There is a weak relationship between them with an absence of in-phase

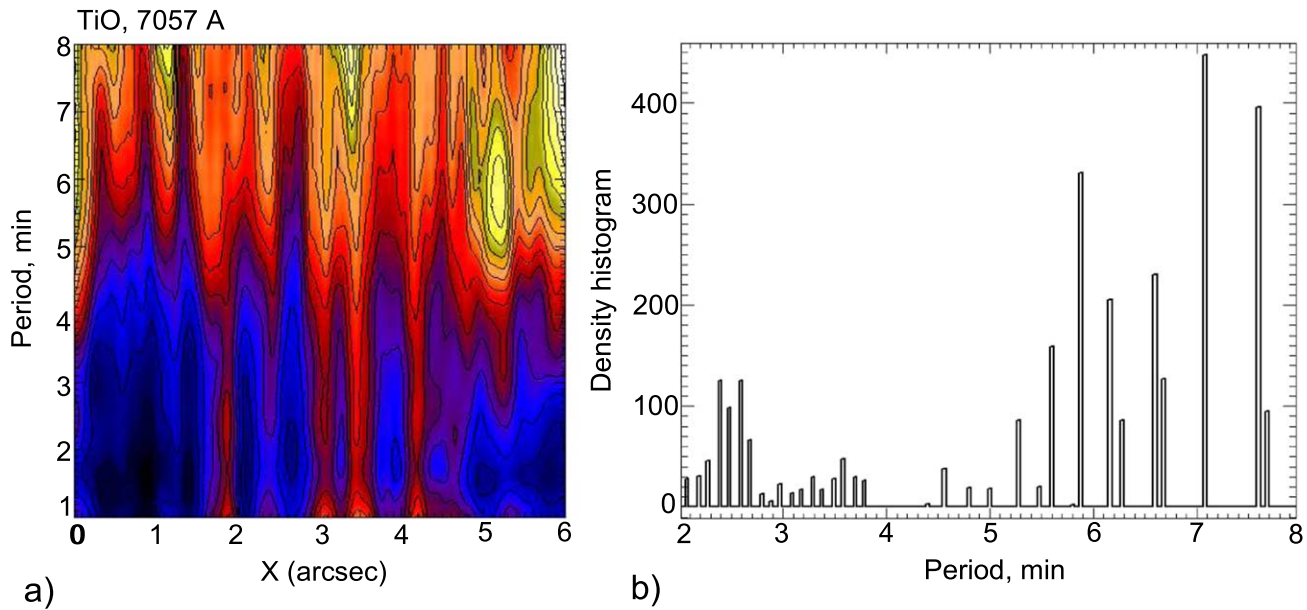


**Figure 8.** (a) 1D spectral distribution of the power oscillations (coordinate–period diagram) of area N1 in the TiO line (7057 Å). (b) Histogram for the spectral density of oscillation period. Period values are in minutes and size in arcseconds.

oscillations. The size of the sources is larger than in the photosphere. The waves propagate radially from the center toward the penumbra along filament sources (Figure 5(c)), whose footpoints look like cells or dots. On the color map the period decreases with distance to the umbral boundary (Figure 5(b)). A similar spatial-frequency dependence was found in Tziotziou et al. (2006, 2007). Zhugzhda & Sych (2014) showed that 3 minutes umbra oscillations are local with the spectrum comprising tens of spectral lines. The oscillations are connected with small sunspot areas. The differences in the spectra of adjacent areas are insignificant.

The low-frequency wave trains (Figure 7) in sufficiently large cells may be interpreted as an increase in wave activity in small umbral areas. Sych et al. (2012) show that the period drifts in the UV range coincide with the appearance of new fine structures in the umbra with maximal power of 3 minutes oscillations. The oscillation period varies with time. We assume that the period drifts can be explained by spatial splitting of propagating waves along the detected fine magnetic tubes with different physical (temperature, density, field strength) and observational (inclination, period) parameters in the framework of the Parker model. The simultaneous wave propagation along magnetic tubes with different cutoff frequencies may explain the observed period drifts.

Oscillations in sunspots are slow waves propagating along magnetic field lines. P-modes occurring penetration into a sunspot transform into fast waves, with conversion into slow waves only at the photosphere level. This process was explained within a model of a vertical field and isothermal atmosphere (Zhugzhda & Sych 2014, 2018). Only large-scale disturbances, comparable with the umbral size, can arise as a result of p-mode conversion into slow waves. This is a wave front that propagates toward the umbral boundary while transforming into running penumbral waves.

Zhugzhda & Sych (2014) show that 3 minutes oscillations in small UDs originate due to exciting oscillations in the subphotospheric resonator for slow waves. The existence of this resonator, predicted by Zhugzhda (1984), was proved

using a thin-tube Roberts approximation (Roberts 2006). Within this model, a mechanism of creating UFs was proposed (Zhugzhda 2018; Zhugzhda & Sych 2019).

We found that the traces from propagating wave fronts, which are spirals or circles (Sych & Nakariakov 2014; Su et al. 2016), do not appear continuously, but consist of many small details that brighten during the transition through the sunspot as UFs. The other observed detail is the existence in the umbra of both 3 and 5 minutes oscillations simultaneously. We assume that both phenomena are a consequence of sunspot inhomogeneity. During propagation, the wave fronts interact with these inhomogeneities. UDs are also inhomogeneities. We can suppose that they are related to the local variations in the magnetic field geometry and accordingly the changes in local cutoff frequency. Such complicated spatial–spectral structure of wave fronts was shown previously (Sych et al. 2012).

### 3.2.2. Photosphere Level

The coordinate–period diagram (Figure 4(a)) showed the increase of oscillation power in the fine umbral structures at the photosphere level. We studied their distribution and parameters in area N1. Similar investigations were performed for the same area at the chromosphere level, and were described above. This allowed comparison of the observational parameters of the identified sources at various heights of the sunspot atmosphere and their relationship.

We calculated the coordinate–period diagram (Figure 8(a)) for the central part of area N1. Similar data preparation for the H $\alpha$  spectral line (Figure 5(a)) was done previously. The obtained diagram shows the broadband sources as extended spatial threads filling the period range from 1 minute up to 8 minutes. The angular size of  $\sim 0''.2$ – $0''.3$  for the identified sources is less than at chromosphere level.

The histogram of spectral density (Figure 8(b)) shows that, as at the chromosphere level (Figure 6(b)), there are two spectral ranges where oscillations are present. The first range is near the  $\sim 3$  minutes weak periodicity, and the other one near  $\sim 5$  minutes with the maximal oscillation power.



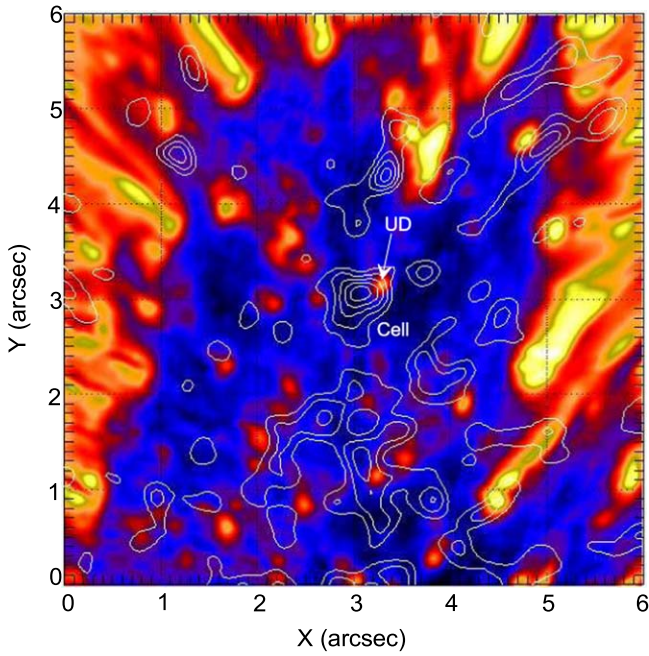


**Figure 9.** Image of the umbra obtained in the TiO line at 18:36 UT. Contours show the location of  $\sim 3$  minutes oscillation sources in  $H\alpha$  at the chromosphere level. Brightness is shown on a logarithmic scale. An arrow indicates the studied UD.

The maximum variation in emission at the photosphere level is observed outside the umbra and related to non-periodic plasma outflow in the sunspot. In the umbra we see the periodic oscillations. These oscillations in various parts of area N1 showed simultaneous temporal changes as standing waves. There is no running wave inside the oscillating areas as at the chromosphere level.

In the umbra we found the separated dots and extended sources as brightenings of some parts of it (Figure 9, background). These bright sources are related to the so-called UDs and widely investigated earlier in a number of papers (Jess et al. 2012; Goodarzi et al. 2016; Ebadi et al. 2017). They exist as both single UDs and UD chains. When comparing the power distribution of 1D oscillations (Figure 8(a)) we found that the umbral sources of vertical threadlike periodicity coincide with the location of the detected UDs on the 2D map (Figure 9). The high-frequency oscillation power here is higher than in the surrounding regions.

We superimposed the map for the  $\sim 3$  minutes periodicity at the chromosphere level on the photospheric image, obtained at 18:36 UT for area N1 (Figure 9). The comparison of the sources at various levels of the sunspot atmosphere shows that the overlying chromospheric sources (denoted by contours) are displaced relative to the photospheric UDs. Their angular size is larger and they have both a compact and an extended shape. The photospheric chains of extended UDs are accompanied by the same chains of UDs at the chromosphere level. Every source in the TiO line corresponds to the source as a cell or a filament in  $H\alpha$ . This dependence indicates that the detected oscillations are probably interconnected among themselves and have a common oscillation source located below, at the photosphere level.

To test the relationship between propagating waves for two UD sources located at different heights, we selected a bright photospheric umbral dot, shown by an arrow in Figure 9, and

the nearest oscillating chromospheric cell, marked by cross in Figure 5(a). We filtered the brightness variations within the 2–4 minutes range to detect periodic oscillations and to compare them. We found that the level of oscillation power in the chromosphere is much bigger than at the photosphere level. The oscillation peaks are displaced relative to one another. The cross-correlation of the two profiles showed a lag of  $\sim 20$  s with a coefficient  $\sim 0.2$ . The obtained lag value agrees with values obtained earlier (Kobanov et al. 2011b) for the time difference of waves propagating at the photosphere–chromosphere levels. The weak level of correlation, which was previously shown in Kobanov et al. (2011a), is probably related to the displacement of sources at different heights relative to one another. Near the investigated cell, we found several pointed UDs that are probably the footpoints of an inclined magnetic tube (or a tube bundle) that expands with height. We observe the upper part of this magnetic structure as an oscillating cell.

Based on the obtained results we can conclude that for the photosphere level, the sunspot oscillations have a broad-band behavior with a low level of high-frequency oscillations in fine umbral structures and strong low-frequency oscillations in the penumbra. Both type of oscillation are related to the global p-mode periodicity (Lites et al. 1982; Lites 1986; Bogdan & Judge 2006). There is strong umbral oscillation damping, which was noted earlier in Chou et al. (2009) and Stangalini et al. (2011) and interpreted as local absorption with decreasing emission. Using helioseismology methods (Braun & Duvall 1990; Nicholas et al. 2004), suppression of the photospheric sunspot oscillations was recorded.

The periodic oscillations fill the whole umbra and are localized with maximal power in cells and fine filaments. We revealed that all oscillate in-phase, as a global standing wave without motion. In Jess et al. (2012) a similar umbral oscillation behavior was referred to as a “drum skin” jitter. In the penumbra, the low-frequency component prevails.

In the umbra there are brightenings that appear as photospheric UDs. An increase in the periodic  $\sim 3$  minutes oscillations is observed, as compared to the surrounding areas (Krishna Prasad et al. 2015; Chae et al. 2017). Those oscillations are hidden mainly in smooth low-frequency brightness variations of UDs.

We may assume that the observed increase in UD oscillations is a result of the intensification of the background p-mode that surrounds UDs. These oscillating areas cause in-phase oscillations and wave motions in UDs. Shelyag et al. (2009) showed that, in the small-scale sources, the magnetic field line curvature and the field strength can result in a significant effect on the propagation of magnetoacoustic waves.

There are spatial differences in localization of the 3 minutes sources for TiO and  $H\alpha$  spectral lines. When comparing their position on the 1D coordinate–period diagrams (Figures 5(a), 8(a)) or a narrowband map (Figure 9), we can see that at the photosphere level the size of UDs is smaller than in the chromosphere. The sources are displaced relative to each other. This agrees well with Jess et al. (2012), where for the 4170 Å continuum,  $H\alpha$  and Ca II 8542 Å core were found from the spatial displacement of the UDs. Such a behavior is probably explained by the geometry of magnetic field lines, where wave propagation is observed. There is a magnetic field inclination relative to the solar normal at the photosphere–chromosphere

levels, which increases the UD size due to the expansion of magnetic tubes with height.

#### 4. Conclusion

We study the fine structure of oscillation sources at different levels of the sunspot atmosphere. For the  $H\alpha$  line (chromosphere level), the  $\sim 3$  minutes oscillations represent a set of numerous independent sources of oscillations with various amplitudes as cells and filaments. The detected sources of small angular size interact weakly among themselves. There are only local oscillations. Each spectral harmonic corresponds to its narrowband source and is linked to the footpoints of elongated filamentary structures as waveguides, visible on the variance map. Their shape varies from pointed in the umbral center to extended in the penumbra. These changes are related to the increase in oscillation period. We show the presence of unstable low-frequency  $\sim 5$  minutes oscillation sources in the umbra located between high-frequency  $\sim 3$  minutes sources without overlap. Their shape is mainly cellular. The temporal dynamics of the  $\sim 3$  minutes oscillations shows a non-monotonic character as low-frequency trains. During the train evolution, the period is observed to drift. Those drifts were described earlier in the UV range (Sych et al. 2012). The drifts are shown only for extended sources with large angular size. A possible explanation for this is instability in the oscillation period of regions of small angular size composing larger sources.

For the 7057 Å (TiO) spectral line (photosphere level), the oscillations have a broadband character, with simultaneous, in-phase temporal variations of the whole umbral region with  $\sim 5$  minutes periodicity. We also found the existence of  $\sim 3$  minutes oscillations in UDs with maximal power. We have shown that the spatial positions of the  $\sim 3$  minutes oscillation sources are displaced at different heights. A possible explanation for this is inclination of the magnetic field lines, along which the waves propagate. The increase in the angular size of the sources at the chromosphere level is associated with the expansion of the magnetic waveguide with height.

The obtained results show that the fine structures of the umbral oscillations as cells and filaments are related to the footpoints of fine magnetic tubes, anchored in the umbra, where the waves are observed to propagate. These processes are reflection of slow magnetoacoustic waves from the subphotospheric level to the corona. The sources' location and wave dynamics indicate a common source as broadband subphotospheric oscillations. It can be assumed that sunspot umbral and penumbral oscillations have different origins. In the umbra this is related to exciting oscillations in the subphotospheric slow-wave resonator. In the penumbra, the origin of the filament components and their increase in angular size are related to increasing magnetic field inclination to the solar normal and to changes in the cutoff frequency of the propagating waves.

This study was supported by the Ministry of Education and Science of the Russian Federation. The authors are grateful to the BBSO team for operating the instrument and performing the basic data reduction, and especially for the open data policy. We thank Dr. N.I. Kobanov for fruitful discussion, and Dr. S.A. Anfinogentov for his assistance in processing the experimental data. The study was performed within the basic

funding from FR program II.16, RAS program KP19-270, and partially supported by the Russian Foundation for Basic Research (RFBR) under grant 17-52-80064 BRICS-a. The BBSO operation is supported by NJIT and US NSF AGS-1821294 grant. GST operation is partly supported by the Korea Astronomy and Space Science Institute and Seoul National University and by the strategic priority research program of CAS with grant No. XDB09000000.

#### ORCID iDs

Robert Sych  <https://orcid.org/0000-0003-4693-0660>

Xiaoli Yan  <https://orcid.org/0000-0003-2891-6267>

#### References

- Balthasar, H., Wiehr, E., & Kueveler, G. 1987, *SoPh*, **112**, 37
- Beckers, J. M., & Tallant, P. E. 1969, *SoPh*, **7**, 351
- Bel, N., & Leroy, B. 1977, *A&A*, **55**, 239
- Bloomfield, D. S., Lagg, A., & Solanki, S. K. 2007, *ApJ*, **671**, 1005
- Bogdan, T. J., & Judge, P. G. 2006, *RSPTA*, **364**, 313
- Braun, D. C., & Duvall, T. L., Jr. 1990, *SoPh*, **129**, 83
- Cao, W., Ahn, K., Goode, P. R., et al. 2011, in ASP Conf. Ser. 437, Solar Polarization 6, ed. J. R. Kuhn et al. (San Francisco, CA: ASP), 345
- Chae, J., Lee, J., Cho, K., et al. 2017, *ApJ*, **836**, 18
- Chou, D.-Y., Yang, M.-H., Zhao, H., Liang, Z.-C., & Sun, M.-T. 2009, *ApJ*, **706**, 909
- de la Cruz Rodríguez, J., Rouppe van der Voort, L., Socas-Navarro, H., & van Noort, M. 2013, *A&A*, **556**, A115
- De Pontieu, B., Erdélyi, R., & De Moortel, I. 2005, *ApJL*, **624**, L61
- De Pontieu, B., Erdélyi, R., & James, S. P. 2004, *Natur*, **430**, 536
- de Wijn, A. G., McIntosh, S. W., & De Pontieu, B. 2009, *ApJL*, **702**, L168
- Ebadi, H., Abbasvand, V., & Pourjavadi, H. 2017, *AN*, **338**, 662
- Goodarzi, H., Koutchmy, S., & Adjabshirizadeh, A. 2016, *Ap&SS*, **361**, 366
- Jain, R., Gascoyne, A., Hindman, B. W., & Greer, B. 2014, *ApJ*, **796**, 72
- Jess, D. B., De Moortel, I., Mathioudakis, M., et al. 2012, *ApJ*, **757**, 160
- Jess, D. B., Reznikova, V. E., Van Doorselaere, T., Keys, P. H., & Mackay, D. H. 2013, *ApJ*, **779**, 168
- Khomenko, E., & Collados, M. 2015, *LRSP*, **12**, 6
- Kiddie, G., De Moortel, I., Del Zanna, G., McIntosh, S. W., & Whittaker, I. 2012, *SoPh*, **279**, 427
- Kneer, F., Mattig, W., & v. Uexkuell, M. 1981, *A&A*, **102**, 147
- Kobanov, N. I., Kolobov, D. Y., Chupin, S. A., & Nakariakov, V. M. 2011a, *A&A*, **525**, A41
- Kobanov, N. I., Kolobov, D. Y., Sklyar, A. A., Chupin, S. A., & Pulyaev, V. A. 2009, *ARep*, **53**, 957
- Kobanov, N. I., Kustov, A. S., Chupin, S. A., & Pulyaev, V. A. 2011b, *SoPh*, **273**, 39
- Krishna Prasad, S., Jess, D. B., & Khomenko, E. 2015, *ApJL*, **812**, L15
- Lites, B. W. 1986, *ApJ*, **301**, 992
- Lites, B. W., White, O. R., & Packman, D. 1982, *ApJ*, **253**, 386
- López Ariste, A., Socas-Navarro, H., & Molodij, G. 2001, *ApJ*, **552**, 871
- Marsh, M. S., Walsh, R. W., & Plunkett, S. 2009, *ApJ*, **697**, 1674
- Nagashima, K., Sekii, T., Kosovichev, A. G., et al. 2007, *PASJ*, **59**, 631
- Nakariakov, V. M., & King, D. B. 2007, *SoPh*, **241**, 397
- Nicholas, C. J., Thompson, M. J., & Rajaguru, S. P. 2004, *SoPh*, **225**, 213
- Reznikova, V. E., & Shibasaki, K. 2012, *ApJ*, **756**, 35
- Reznikova, V. E., Shibasaki, K., Sych, R. A., & Nakariakov, V. M. 2012, *ApJ*, **746**, 119
- Roberts, B. 2006, *RSPTA*, **364**, 447
- Rouppe van der Voort, L. H. M., Rutten, R. J., Sütterlin, P., Sloover, P. J., & Krijger, J. M. 2003, *A&A*, **403**, 277
- Schüssler, M., & Vögler, A. 2006, *ApJL*, **641**, L73
- Settele, A., Staude, J., & Zhugzhda, Y. D. 2001, *SoPh*, **202**, 281
- Shelyag, S., Zharkov, S., Fedun, V., Erdélyi, R., & Thompson, M. J. 2009, *A&A*, **501**, 735
- Socas-Navarro, H., Trujillo Bueno, J., & Ruiz Cobo, B. 2000, *Sci*, **288**, 1396
- Stangalini, M., Del Moro, D., Berrilli, F., & Jefferies, S. M. 2011, *A&A*, **534**, A65
- Su, J. T., Ji, K. F., Cao, W., et al. 2016, *ApJ*, **817**, 117
- Sych, R., Karlický, M., Altyntsev, A., Dudík, J., & Kashapova, L. 2015, *A&A*, **577**, A43

- Sych, R., & Nakariakov, V. M. 2014, [A&A](#), **569**, [A72](#)
- Sych, R., Nakariakov, V. M., Karlicky, M., & Anfinogentov, S. 2009, [A&A](#), **505**, [791](#)
- Sych, R., & Wang, M. 2018, [A&A](#), **618**, [A123](#)
- Sych, R., Zaqarashvili, T. V., Nakariakov, V. M., et al. 2012, [A&A](#), **539**, [A23](#)
- Sych, R. A., & Nakariakov, V. M. 2008, [SoPh](#), **248**, [395](#)
- Sych, R. A., Nakariakov, V. M., Anfinogentov, S. A., & Ofman, L. 2010, [SoPh](#), **266**, [349](#)
- Torrence, C., & Compo, G. P. 1998, [BAMS](#), **79**, [61](#)
- Tsiropoula, G., Alissandrakis, C. E., & Mein, P. 2000, [A&A](#), **355**, [375](#)
- Turova, I. P., Teplitskaia, R. B., & Kuklin, G. V. 1983, [SoPh](#), **87**, [7](#)
- Tziotziou, K., Tsiropoula, G., Mein, N., & Mein, P. 2006, [A&A](#), **456**, [689](#)
- Tziotziou, K., Tsiropoula, G., Mein, N., & Mein, P. 2007, [A&A](#), **463**, [1153](#)
- Wang, T. J., Ofman, L., & Davila, J. M. 2009, in ASP Conf. Ser. 415, The Second Hinode Science Meeting: Beyond Discovery-Toward Understanding, ed. B. Lites et al. (San Francisco, CA: ASP), [28](#)
- Wittmann, A. 1969, [SoPh](#), **7**, [366](#)
- Yuan, D., Sych, R., Reznikova, V. E., & Nakariakov, V. M. 2014, [A&A](#), **561**, [A19](#)
- Yuan, Y., Shih, F. Y., Jing, J., Wang, H., & Chae, J. 2011, [SoPh](#), **272**, [101](#)
- Zhugzhda, I. D. 1984, [MNRAS](#), **207**, [731](#)
- Zhugzhda, I. D., & Dzhililov, N. S. 1984, [A&A](#), **133**, [333](#)
- Zhugzhda, Y., & Sych, R. 2018, [RAA](#), **18**, [105](#)
- Zhugzhda, Y. D. 2018, [AstL](#), **44**, [331](#)
- Zhugzhda, Y. D., & Sych, R. A. 2014, [AstL](#), **40**, [576](#)
- Zhugzhda, Y. D., & Sych, R. A. 2019, [AstL](#), **45**, [177](#)